ELSEVIER

Journal of Molecular Catalysis A: Chemical 145 (1999) 169–181

JOURNAL OF MOLECULAR CATALYSIS A: CHEMICAL

www.elsevier.com/locate/molcata

Characterization of Ni, Mo and Ni–Mo catalysts supported on alumina-pillared α-zirconium phosphate and reactivity for the thiophene HDS reaction

J. Mérida-Robles, E. Rodríguez-Castellón, A. Jiménez-López *

Departamento de Química Inorgánica, Cristalografía y Mineralogía, Facultad de Ciencias, Universidad de Málaga, 29071 Málaga, Spain

Received 19 May 1998; accepted 19 November 1998

Abstract

A series of fluorinated alumina pillared α-zirconium phosphate supported with nickel, molybdenum and nickel–molybdenum sulfide catalysts was prepared in order to investigate the use of an alumina-pillared material, i.e., an alumina diluted within another inorganic matrix, as a support of sulfide catalysts. The catalysts were prepared by impregnation, with loadings of 4, 8, 12 wt.% of Ni; 13 wt.% of Mo and 2.1–9, 3–13 wt.% of Ni–Mo followed by calcination at 673 K. Sulfidation was performed at 673 K for 2 h. They were characterised by X-ray diffraction (XRD), temperature-programmed reduction (TPR) and X-ray photoelectron spectroscopy (XPS). The set of data indicated that in the Ni-based catalysts a fraction of the loaded Ni^{2+} interacts with the support and cannot be sulfided at 673 K. However, a total sulfidation of Ni^{2+} is reached in the NiMo-based catalysts. The Ni $2p_{3/2}$ binding energy (B.E) of Ni–Mo sulfided catalysts shifted to higher values (> 1 eV) with respect to those observed in Ni-based catalysts suggesting the existence of different environments for Ni in these materials. The catalysts can be easily regenerated by treatment with 5% (v/v) O_2/N_2 mixture at 673 K without noticeable loss of activity. The catalysts exhibited a high activity and stability for thiophene HDS particularly the NiMo catalysts due to the promotion of Ni for Mo-based catalysts.

Keywords: Pillared; Alumina; Nickel; Molybdenum; HDS; Catalysis; Zirconium phosphate

1. Introduction

Hydrodesulfurization is one of the most important reactions in petroleum refining processes for removing sulfur components in the feedstock. These components present several important problems such as pollution of the environment through increased SO_2 emissions, corrosion of materials with which they have contact, poisoning of reforming catalysts, and cause petroleum products to have undesirable odors and burning characteristics. In recent years, growing environmental concerns have coupled with dwindling fossil fuel reserves to increase the interest in HDS catalysts for pro-

* Corresponding author

1381-1169/99/$ - see front matter
PII: S1381-1169(99)00048-5

ducing cleaner fuels from lower quality feedstocks.

Among the numerous catalytic formulae investigated, the most commonly used are CoMo and NiMo mixed sulfides supported on alumina. The results of intensive research [1–11] show that in the final oxidic or precursor state various degrees of chemical interaction exist between the amorphous alumina and the transition metal oxides. Some of the formed phases are very stable and resist sulfidation. Studies on nickel sulfide catalysts have concluded that supports, such as Al_2O_3, interact strongly with Ni^{2+} cations which impede their sulfidation. X-ray photoelectron spectroscopy (XPS) and X-ray diffraction (XRD) revealed the presence of the phase $NiAl_2O_4$ on catalysts, which is formed on calcination at high temperatures [12–15].

Metal–alumina interactions may be weakened by using carriers such as alumina-pillared compounds, where the aluminium oxide is diluted within a layered inorganic matrix. In these systems, alumina nanoparticles induce permanent porosity by propping open the layers of the host, thus making the resulting solids suitable to be used as supports. In this way Occelli and Rennard [16] applied a pillared bentonite as a support for an Ni–Mo catalyst for hydrogenation-hydrocracking of vacuum gasoil feedstocks, and Kloprogge et al. [17] supported nickel sulfide on alumina pillared montmorillonite which exhibits high activity for DHS of thiophene. In previous works, we described the preparation and surface properties of fluorinated alumina α-zirconium phosphate materials [18] as well as their use as supports for preparing nickel catalysts. These catalysts proved to be highly active for the hydrogenation of benzene with imperceptible deactivation [19]. The aim of the present work was thus to study the effect of these pillared structures on sulfidation and activity of supported-nickel, molybdenum and nickel–molybdenum sulfide catalysts for the HDS reaction. For this purpose, the materials were characterized using XRD, XPS, thermoprogrammed reduction (TPR) with H_2 and, finally, the hydrodesulfurization of thiophene has been chosen to probe the activity of these different supported catalysts.

2. Experimental

The support chosen was a fluorinated alumina pillared α-zirconium phosphate, prepared as described elsewhere [18] and calcined at 673 K for 6 h. The calcined material, with empirical formulae: $Zr[Al_{3.39}O_{1.12}(OH)_{1.60}F_{4.90}]H_{0.57}(PO_4)_2$, hereafter referred as AlZrP-1. Ni^{2+} and $Mo^{(VI)}$ were incorporated into the supports using the incipient impregnation method with ethyl alcohol solutions of $Ni(NO_3)_2$ corresponding to nickel loadings of 4, 8 and 12 wt.% and aqueous solutions of ammonium molybdate $[(NH_4)_6Mo_7O_{24}\cdot 4H_2O]$ corresponding to 13 wt.%. Another set of catalysts containing both nickel and molybdenum were prepared by successive impregnations with loadings of 2.1–9 wt.% and 3–13 wt.% Ni–Mo. All samples were then dried at 333 K and calcined at 673 K for 5 h.

The TPR of thermally treated samples was performed between 313 and 973 K, using a flow of Ar/H_2 (40 cm^3/min, 10% of H_2) and heating at 10 K/min. The water produced in the reduction was eliminated by passing the gas flow through a cold finger (193 K). The consumption of reductor was controlled by an online gas chromatrograph provided with a TC detector.

Powder diffraction patterns (XRD) of samples were performed with a Siemens D501 diffractometer, provided with a graphite monochromator and using Cu $K\alpha$ radiation. XPS analysis were obtained with a Physical Electronics 5700 instrument with a Mg $K\alpha$ X-ray excitation source ($h\nu = 1253.6$ eV) and hemispherical electron analyser. Accurate (± 0.1 eV) binding energies (BEs) were determined with respect to the position of the C 1s peak at 284.8 eV. Mol percentages of P, O, Zr, Ni, Mo and S were determined. The measured peaks areas

(P 2p, O 1s, Zr 2p, Ni 2p, Mo 3d and S 2p) (counts s^{-1}) of the fits were multiplied with the corresponding sensitivity factors [20]. The residual pressure in the analysis chamber was maintained below 10^{-9} Torr during data acquisition. The catalysts were always handled under hexane after the sulfidation to keep them under air-free conditions.

The catalysts were tested in the thiophene hydrodesulfurization reaction at 673 K, using an automatic microcatalytic flow reactor under atmospheric pressure. The catalysts were supported between quartz wool in a quartz tube reactor; the catalyst charge used was 0.2 g without dilution. The catalysts were heated (673 K) under He flow and then sulfided in situ in a flow of 60 cm^3/min H_2S/H_2 (10% H_2S) using the following temperature programme: 10 K/min increase from r.t. to 673 K and keeping the catalysts for 1 h at 673 K. After sulfidation, the gas flow was switched to the reaction mixture; a hydrogen flow of 50 cm^3/min containing 4.0 mol.% thiophene. The contact time was 0.15 g s/mmol and catalysts did not show diffusion restrictions. The reactor effluents were sampled via a microvolume sampling valve and injected into a gas chromatogragh equipped with a flame ionization detector and a capillary column (TRB-1). Based on conversion data, and assuming that reactions are pseudo-first order, reaction rate constants (K_{HDS} and K_{HYD}) were calculated.

3. Results

3.1. Characteristics of the support and calcined precursor samples

A fluorinated alumina pillared α-zirconium phosphate support designated as AlZrP-1 (Al_2O_3, 29.3 wt.%; $S_{BET} = 184\ m^2/g$) was used in this study. This material displays a mixed porosity, essentially within the range of mesoporous but with a micropore contribution of $\approx 0.1\ cm^3/g$, and containing acid sites (1.5 mmol NH_3/g determined by NH_3 thermal programmed desorption), mainly of Lewis type, which are active in the dehydration of isopropyl alcohol [18].

Calcination of precursor samples at 673 K gave rise to the formation of Ni, Mo and Ni–Mo oxides supported on the pillared materials. The presence of NiO and MoO_3 on the surface of the supports was confirmed by XRD and XPS analysis. The characteristic diffraction lines of NiO appear at 2.41, 2.09 and 1.48 Å for the

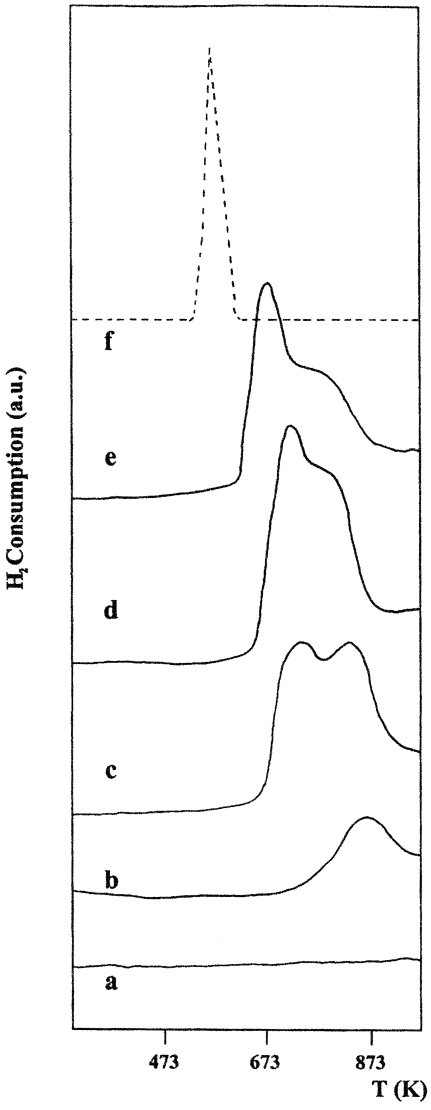

Fig. 1. TPR profiles of NiO supported materials with different Ni percentages (wt.%): (a) 0%; (b) 4%; (c) 8%; (d) 12%; (e) 12% (623 K); (f) unsupported NiO.

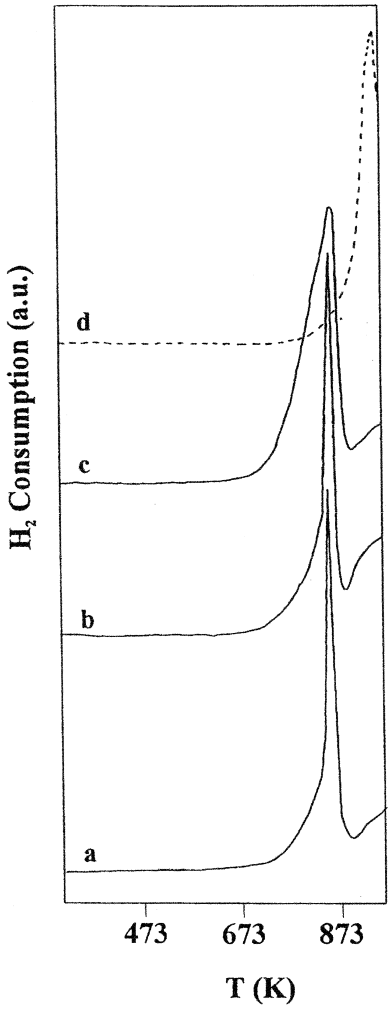

Fig. 2. TPR profiles of NiMo and Mo oxides supported materials: (a) Ni–Mo 2.1–9%; (b) Ni–Mo 3–13%; (c) Mo 13%; (d) unsupported MoO_3.

Ni-based materials, and their intensities increased with nickel loading, as expected. The XRD patterns of samples containing Mo and Ni–Mo oxides only show the peaks corresponding to MoO_3 at 3.81, 3.46 and 3.26 Å. This means that Ni^{2+} is highly dispersed in Ni–Mo precursors.

The TPR profiles of NiO supported on alumina-pillared α-zirconium phosphate are shown in Fig. 1. The existence of several defined ranges of H_2 consumption in the TPR profiles pointed to the presence of more than one Ni^{2+} species in calcined precursors with different degrees of metal–support interaction. It is assumed that a stronger interaction with the support results in a higher reduction temperature. The samples with maximum loading of Ni and calcined at the lower temperature of 623 K appears to be easily reducible with a maximum at 673 K.

Although the reduction process of Mo(VI) to Mo(0) takes place in two steps at 893–925 K and 1075 K [21], the TPR profiles of Mo and NiMo calcined precursors (Fig. 2) only include the reduction step from Mo(VI) to Mo(IV) in as

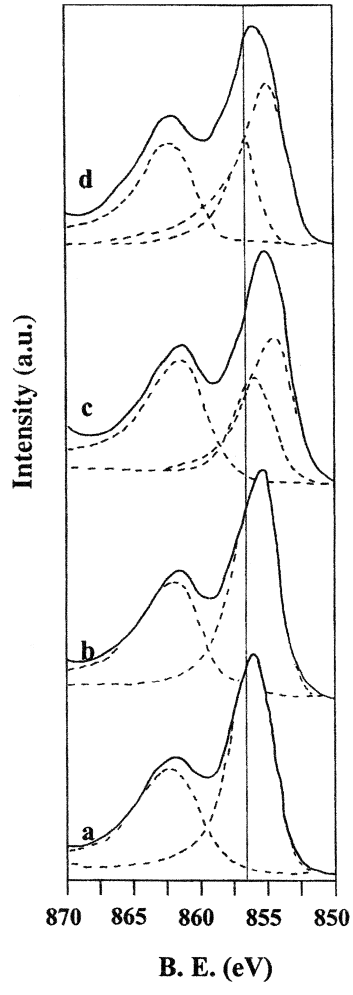

Fig. 3. Ni $2p_{3/2}$ spectra of NiO supported materials: (a) 4%; (b) 8%; (c) 12%; (d) 12% (623 K).

much as sulfidation of molybdenum oxide usually leads to the formation of MoS_2. In general, the low content of Ni in NiMo materials does not seem to affect the reducibility of MoO_3. In contrast to supported nickel oxides, the molybdenum ones present the reduction peak at a temperature lower than that of the bulk MoO_3 and the small difference in temperature is indicative of a weak interaction of the molybdenum oxide with the support.

The degree of interaction of the Ni, Mo and NiMo oxides with the support was studied by XPS. The Ni $2p_{3/2}$ XPS spectra (Fig. 3) show a main peak, characteristic of Ni^{2+}, which shifts to lower BE values from 856.1 to 855.1 eV and becomes wider at higher nickel loading. In samples with loading higher than 8%, this peak could be decomposed into two components, one centered at 854.1 eV and the other at 856.1 eV (Table 1). Taking into account that the BE for un-supported NiO is 853.5 eV, the peak at 854.1 eV may be assigned to Ni^{2+} in octahedral sites of the supported NiO structure, and the peak at 856.1 eV may then be associated with Ni^{2+} in tetrahedral positions of a spinel-like structure of Ni–Al oxide, created as a result of the solid-state diffusion of Ni^{2+} into the lattice during the calcination process [12,22]. When the calcination temperature is lower (623 K), the intensity of the low energy peak increases as a consequence of the decreased diffusion of Ni^{2+}

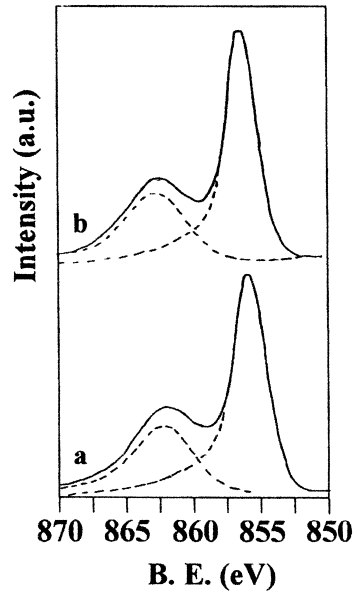

Fig. 4. Ni 2 $p_{3/2}$ spectra of NiMo oxide supported materials: (a) Ni–Mo 2.1–9%; (b) Ni–Mo 3–13%.

Table 1
Binding energy (BE), surface atomic ratio as determined by XPS analysis

Ni (wt.%)	Mo (wt.%)	BE (eV)		Atomic ratio on surface				
		Ni $2p_{3/2}$	Mo 3d	Ni/Zr	Mo/Zr	S/Mo	$S/Ni_{sulfided}$	$\%Ni_{sulfided}$
Un-sulfided catalysts								
4		855.9		0.71				
8		855.7		0.98				
12		856.1–854.7		1.48				
12 (623 K)		855.3–853.5		2.03				
2.1	9	855.4	232.6–235.5	0.42	3.43			
3	13	855.5	232.5–235.5	0.96	5.78			
0	13		232.6–235.7		4.01			
Sulfided catalysts								
4		855.7–851.8		0.50			1.06	22.6
8		855.6–851.5		0.85			1.05	30.6
12		855.3–851.3		1.01			1.47	34.3
12 (623 K)		855.4–852.4		1.49			1.30	33.6
2.1	9	852.7	229.1–232.3	0.67	2.98	1.94		100.0
3	13	852.8	229.1–232.3	1.16	3.82	1.98		100.0
0	13		229.2–232.3		3.01	1.68		

into the support (Fig. 3, curve d). The peak located at 862 eV, which essentially remains in the same position corresponds to the shake-up satellite structure of Ni^{2+} [23]. The Ni $2p_{3/2}$ spectra for the samples containing NiMo oxides (Fig. 4) show a weak peak with BE values about 855.5 eV, this value is halfway between those found for Ni supported precursors. This new BE value suggests that the environment of Ni^{2+} ions in NiMo materials is different from that in supported nickel oxides. The XPS Mo 3d spectra (Fig. 5) for the samples containing MoO_3 and mixed oxides of NiMo show the MoO_3 characteristic doublet, Mo $3d_{5/2}$ and Mo $3d_{3/2}$ with BE values of 232.2 and 235.5 eV, respectively. The Mo/Zr surface atomic ratio has been obtained from the XPS superficial analysis. This ratio, for samples with the same loading of Mo, is higher in the samples which contain NiMo than in those having only Mo. This means that the dispersion of MoO_3 is higher in materials containing Ni as promoter atoms (Table 1).

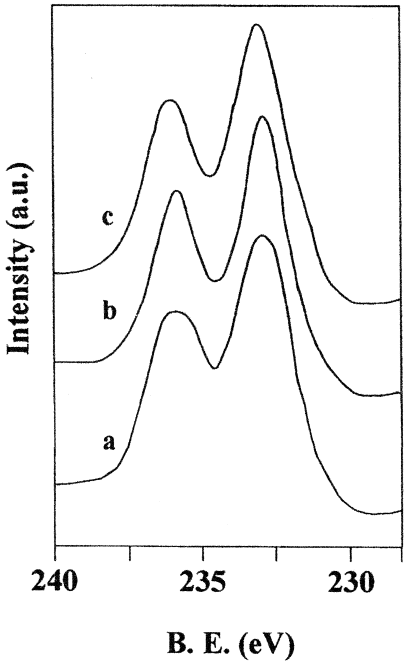

Fig. 5. Mo 3d spectra of Mo and NiMo oxide supported materials: (a) Mo 13%; (b) Ni–Mo 2.1–9%; (c) Ni–Mo 3–13%.

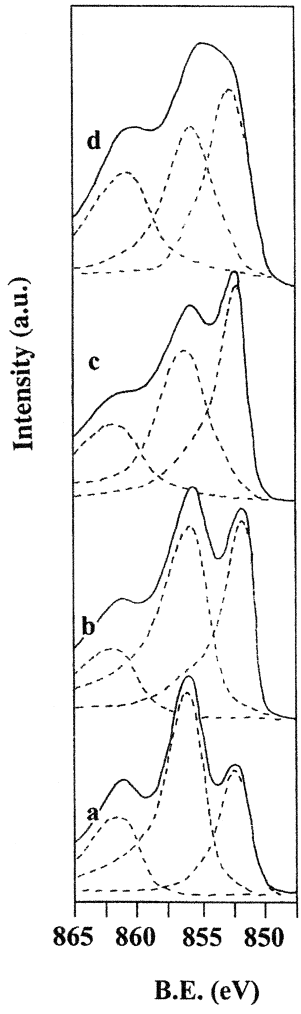

Fig. 6. Ni $2p_{3/2}$ spectra of supported Ni sulfide catalysts: (a) 4%; (b) 8%; (c) 12%; (d) 12% (623 K).

3.2. Sulfided catalysts

Evidence of formation of metallic sulfides on the support surface was again provided by XRD and XPS analyses. The XRD patterns of sulfided Ni–AlZrP catalysts show the presence of low crystallinity sulfide phases for loading higher than 8% with very weak diffraction lines at 1.71, 1.97 and 2.97 Å corresponding to NiS. This phase is usually found in catalysts where strong nickel–support interactions occur [24,25]. Neither phase was detected in 4 wt.% Ni sample, suggesting that, Ni^{2+} should be extremely

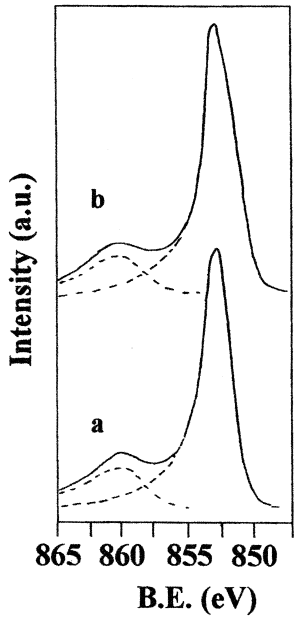

Fig. 7. Ni $2p_{3/2}$ spectra of supported NiMo sulfide catalysts: (a) Ni–Mo 2.1–9%; (b) Ni–Mo 3–13%.

dispersed in this case also and strongly interacting with the support. In the XRD patterns of Mo and NiMo catalysts, the diffraction peaks corresponding to the MoS_2 phase at 2.03 and 2.35 Å are hardly visible. Also the absence of diffraction lines of nickel sulfide in the sulfided NiMo–AlZrP catalysts may indicate that Ni^{2+} could be inserted into the structure of MoS_2 forming a solid solution.

The BE values, Ni/Zr and Mo/Zr surface atomic ratios for samples before and after sulfidation are compared in Table 1. Since the BE of Zr $3d_{5/2}$ and P 2p core electrons were practically constant with values of 183.3 and 134.1 eV, respectively, and the P/Zr atomic ratio was maintained close to the theoretical value, P/Zr = 2, it may be inferred that the impregnation–calcination–sulfidation processes did not significantly alter the host framework. The Ni $2p_{3/2}$ XPS spectra of sulfided Ni catalysts (Fig. 6) show a new peak at 851.3–851.9 eV, which is indicative of the presence of sulfided nickel, together with another signal in the range 855.0–855.7 on the same position that the highest energy peak in the precursor and assigned to Ni in the form of $NiAl_2O_4$. This means that a fraction of Ni in the oxide form which strongly interacts with the support it cannot be sulfided at 673 K.

The BE of Al 2p core electrons in the precursor is close to 74.9 eV and is also shifted to higher energy values (75.4 eV) in the sulfided samples, probably as a consequence of the Ni^{2+}-alumina pillar interaction. From XPS data, percentages of Ni^{2+} sulfidation on the integrated peak area of nickel sulfide to the entire Ni peak area (including the satellite peak) has been evaluated. By this method, the percentages of sulfided nickel were lower than 35%. A decrease in the surface Ni/Zr ratio was observed in nickel supported catalysts after sulfidation, attributed to the agglomeration of particles forming nickel sulfide. The $S/Ni_{sulfided}$ surface atomic ratios (Table 1) point to the presence of the NiS phase in these catalysts, which is in agreement with the XRD data.

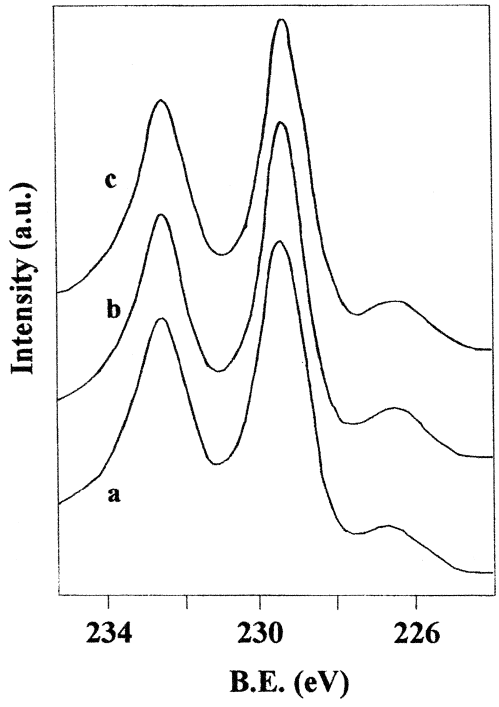

Fig. 8. Mo 3d spectra of supported Mo and NiMo sulfide catalysts: (a) Mo 13%; (b) Ni–Mo 2.1–9%; (c) Ni–Mo 3–13%.

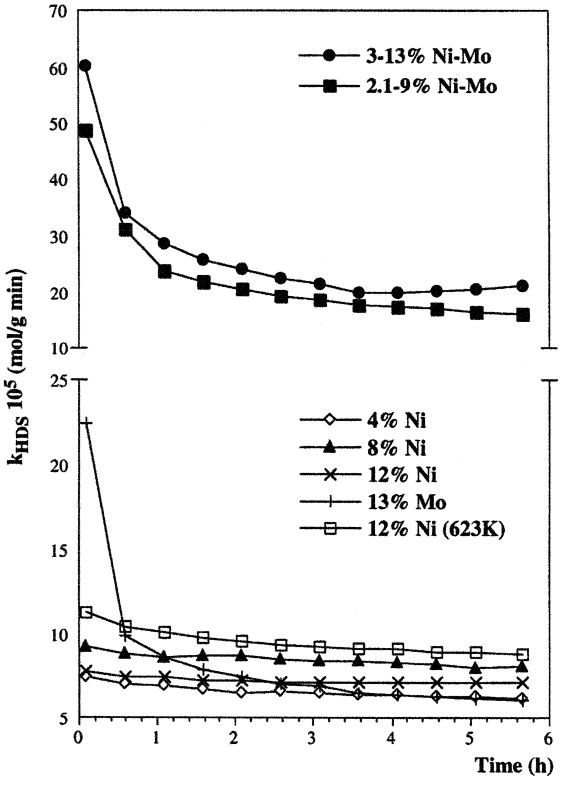

Fig. 9. Plots of K_{HDS} vs. time on-stream for supported Ni, Mo and NiMo sulfide catalysts.

The Ni $2p_{3/2}$ spectra of sulfided NiMo–AlZrP catalysts (Fig. 7) show a single signal at ca. 852.7 eV (Table 1) indicating that Ni^{2+} is completely sulfided and therefore the environment of this ion in the NiMo calcined precursors is different from that of the Ni based materials. It is possible that Ni^{2+} ions are embedded in the structure of supported molybdenum oxide and therefore the interaction with the support, if any, is weak. All sulfided Ni and NiMo catalysts exhibit a BE of S 2p value close to 162.1 eV.

Fig. 8 shows the Mo 3d and S 2s region of the XPS spectra of sulfided catalysts based on Mo and NiMo. All catalysts exhibit the typical Mo $3d_{5/2}$ and Mo $3d_{3/2}$ doublet (well defined) at 229.1 ± 0.1 and 232.3 ± 0.1 eV, respectively, characteristic of MoS_2 species [26–28], and a small shoulder at lower BE (226.5 eV) attributed to S 2s [26,27]. As no significant differences in the position of the bands between both types of the catalysts of Mo were observed the nature of the Mo species may be essentially the same in the catalysts based on Mo and NiMo, viz. MoS_2 species.

The surface Mo/Zr atomic ratio increases with the Mo content (Table 1). For samples with the same Mo percentage, this ratio is higher in NiMo than in Mo catalysts, indicating a higher dispersion of Mo on the surface of the former. The surface S/Mo atomic ratios for NiMo–AlZrP catalysts were very close to 2 which is consistent with the formation of MoS_2 on the catalysts surface and are higher than that observed on Mo catalyst indicating a higher sulfur content.

3.3. Thiophene HDS

The thiophene HDS model reaction has been used to establish the performance of the sulfided Ni, Mo and NiMo–AlZrP catalysts. K_{HDS} values are plotted vs. time on-stream in Fig. 9 and summarised in Table 2 for 5 and 330 min of

Table 2
Pseudo-first-order rate constants for HDS of thiophene and HYD of butene

Ni (wt.%)	Mo (wt.%)	$K_{HDS} \cdot 10^5$ (mol/g min)		$K_{HYD} \cdot 10^5$ (mol/g min)	K_{HYD}/K_{HDS}
		5 min	330 min	330 min	330 min
4		7.50	6.22		
8		9.24	8.16		
12		7.75	7.15		
12 (623 K)		11.39	8.42		
2.1	9	48.53	16.01	4.68	0.30
3	13	60.37	21.23	4.34	0.20
0	13	22.50	6.07	7.80	1.28

reaction. As can be seen, both Ni and Mo catalysts show quite similar activities especially after 330 min of reaction. The sulfided Ni–AlZrP catalysts show quite similar K_{HDS} values regardless of the Ni content, temperature of decomposition of the precursors, etc., although the most active is that with 12% Ni loading and calcined at 623 K which exhibits a K_{HDS} value of 8.42×10^{-5} mol/g min after 330 min on stream. These catalysts present low deactivation. In contrast the sulfided Mo–AlZrP catalysts, which initially display a high thiophene HDS activity, undergo a strong deactivation during the first 30 min then showing a similar activity to sulfided Ni–AlZrP catalysts. The sulfided NiMo–AlZrP catalysts show a much higher HDS activity than the sulfided Ni and Mo–AlZrP catalysts, which is attributed to the promoting effect of Ni^{2+} ions in the mixed NiMo sulfided materials.

The catalytic behaviour for the thiophene HDS reaction of a calcined precursor and the corresponding sulfided NiMo–AlZrP material is compared in Fig. 10. Although both types of catalysts reached a similar steady-state, their initial catalytic behaviour was completely different. So, the sulfided catalyst undergoes a strong deactivation whereas the catalytic activity of non-sulfided catalyst initially increased up to a maximum value and then smoothly decreased. This fact suggests that in situ sulfidation of the latter took place during the HDS reaction.

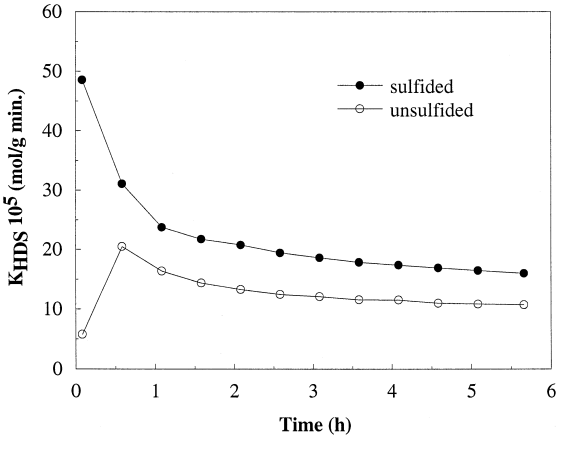

Fig. 10. Variation of K_{HDS} vs. time on-stream for the sulfided and non-sulfided Ni–Mo 2.1–9% catalysts.

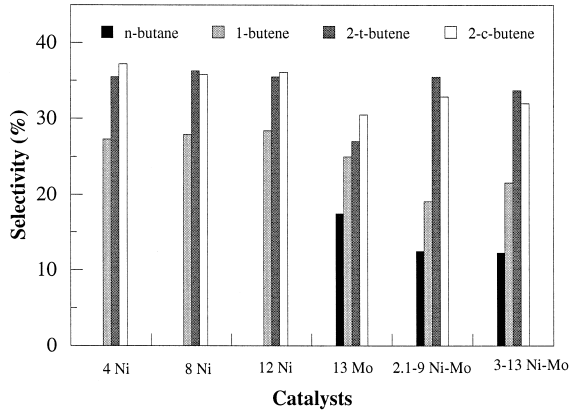

Fig. 11. Selectivity of the supported Ni, Mo and NiMo sulfided catalysts for the thiophene HDS reaction products.

The selectivities of the products of reaction identified by gas chromatography (*n*-butane, 1-butene, *cis*- and *trans*-butene) are shown in Fig. 11. In contrast to the NiMo and Mo catalysts, no *n*-butane was formed on the sulfided Ni–AlZrP. K_{HYD}/K_{HDS} is summarized in Table 2. K_{HYD} is higher for the sulfide Mo–AlZrP catalysts than for the NiMo–AlZrP ones.

4. Discussion

According to TPR profiles of nickel oxide supported materials, the reduction temperature of Ni^{2+} on the surface of fluorinated alumina pillared materials is, in all cases, higher than that corresponding to the un-supported NiO (616 K). XPS data and TPR profiles suggest that Ni^{2+} is present in, at least, two different environments in all the calcined precursors, i.e., forming part of the supported NiO network and as dispersed ions in the alumina framework. H_2 consumption at very high temperature is indicative of the existence of highly dispersed Ni^{2+} strongly interacting with the support. The formation of NiO and Ni–Al spinel oxide has been reported for several nickel catalysts supported

on alumina [11,12,23,29]. These species fixed to the support differ in reducibility and their relative concentration depend on the nickel content, the nature of the support, and the calcination temperature [12–15]. According to the literature [30], Ni^{2+} in a spinel-like structure is more difficult to reduce or sulfide, in consequence the high-temperature TPR peak(s) might be tentatively associated with this species, i.e., $NiAl_2O_4$. The lower-temperature TPR peak(s) may be associated with NiO, which interacts to a lesser extent with the support. On increasing nickel loading the amount of deposited NiO increases and the interaction of the outer NiO overlayer with the support decreases. Thus the corresponding TPR peak shifts to a lower temperature at a high nickel percentage (12 wt.%). The low reducibility of nickel as related to its high dispersion has also been observed in other systems like Ni^{2+}-Y zeolites, where reduction and agglomeration of Ni^{2+} are very difficult [31,32]. The XPS analysis of the Ni-based calcined precursors confirms the presence of more than one kind of supported Ni^{2+} species (BEs at 854.1 and 856.1 eV). XPS data revealed that only the fraction of Ni^{2+} which weakly interacts with the support (BE at 854.1 eV) could be sulfided, because the peak at high BE of Ni^{2+} ($\sim$ 856 eV) remains unchanged. XRD data, with weak diffraction lines at 1.71, 1.97 and 2.97 Å, in samples with Ni loading higher than 8%, point to the thermodynamically most stable nickel sulfide phase, NiS [33,34] was formed on sulfiding Ni catalysts. It is known that strong metal–support interactions give rise to the appearance of the NiS phase, whilst Ni_3S_2 phase is preferentially formed in systems with weak metal–support interactions (e.g., carbon or silica) [35,36]. Consequently the presence of NiS in sulfided Ni catalysts is another indication that, at least a fraction of the Ni^{2+} species strongly interacts with the support, as deduced by TPR-H_2 and XPS analyses. The surface S/Ni atomic ratio obtained by XPS for impregnated samples ranged between 1.05 and 1.47. These values were higher than that corresponding to the Ni_3S_2 phase and thus the formation of this phase may be ruled out.

The loading of Mo in Mo and NiMo catalysts was ranged between 3 and 4.3 Mo atom/nm^2, since this species is highly dispersed on the support as a monolayer [37]. XRD patterns of NiMo calcined precursors show only the signals corresponding to MoO_3, but after sulfidation no peak corresponding to MoS_2 is observable. The absence of separate nickel sulfide phases in the sulfided NiMo catalysts is attributed to Ni which may be incorporated in small amounts into the MoS_2 structure. In fact, the XPS analysis indicates that the environment of Ni in the sulfided NiMo-catalysts (BE = 852.7 eV) is different from that in sulfided Ni catalysts (851.3–851.9 eV). Moreover, a total sulfidation of Ni^{2+} ions was only possible for NiMo-calcined precursors, which could be explained by the fact that Ni^{2+} ions were preferentially incorporated into the MoO_3 structure before sulfidation and hence no interaction with the support would be expected in this case. A square pyramidal arrangement of Ni^{2+} ions within the MoS_2 framework, similar to that of the millerite structure, has been proposed [38–41] and confirmed later by EXAFS spectroscopy [35]. The shift of the XPS signal Ni $2p_{3/2}$ at higher BE values in NiMo materials with respect to the Ni ones may be related to the presence of Ni atoms in this particular coordination [42–44] in which nickel exhibits a lower coordination number than in the nickel sulfide [35].

The Mo 3d and S 2p BEs were about the same as the sulfide forms of both monometallic and bimetallic Ni–Mo catalysts but the dispersion of the MoS_2 phase is affected by the addition of Ni atoms as promoter. The dispersion is higher for the catalysts containing Ni promoter atoms, as deduced for the Mo and Ni–Mo with the same content of molybdenum from the surface Mo/Zr atomic ratios which are higher for the sulfided NiMo catalysts (Table 1).

In this study, thiophene was used for the characterisation of sulfided catalysts. The cat-

alytic behaviour displayed by non-sulfided NiMo materials suggests that selfsulfidation by means of the S of thiophene occurs (Fig. 10). This seems to justify the mechanism of hydrodesulfurization proposed by Kabe et al. [45–48], who concluded that sulfur in the reactive (thiophene) is not directly released as hydrogen sulfide but accumulated on the catalysts. After reaction, complete sulfidation of the catalysts was detected by XPS analysis, with BE values of Ni and Mo being in the range of the sulfided forms.

The Ni-based catalysts show a promising value (between 6×10^{-5} to 8×10^{-5} mol/g min) K_{HDS} and do not exhibit deactivation. At a lower temperature of calcination (623 K) the catalyst with the highest Ni loading and sulfided at 673 K shows the maximum activity with a K_{HDS} value close to 10^{-4} mol/g min in good agreement with the maximum found value for sulfidation (Table 2). These results seem indicate that there are special interactions between the nanoparticles of alumina and nickel sulfide which lead to a high dispersion of the active phase and, therefore, to a significant activity. Furthermore, the catalysts do not show deactivation because the acidity of the support is only of Lewis type, and as a consequence of this fact, no formation of coke is observed. In contrast, the Mo catalysts are quickly deactivated, which could be originated from the presence of coordination vacancies on the edges of MoS_2 crystallites in agreement with the low observed S/Mo ratio by XPS for this catalyst (Table 1). H_2S molecules may occupy these vacancies and act as Brönsted acid sites which provoke the formation of coke and consequently a drastic decrease of the catalytic activity [49] by blocking the pores and active sites.

The sulfided NiMo–AlZrP catalysts displayed the highest activity for this reaction, due to the promotion effect of Ni. XPS analysis indicated that this cation was incorporated to the MoS_2 network. After an initial deactivation of the catalyst during the first hour, the activity remains almost constant for a long time. This deactivation is not related with the support, because it is produced by the Brönsted acid centres originated on Mo atoms during the sulfidation process, and it is less than that observed for the MoS_2 catalyst, because the formation of these acid sites is only associated with Mo [36,40,41]. The HDS activity of sulfided NiMo–AlZrP catalysts could be related to the existence of sulfur vacancies (uncoordinated sites) on molybdenum. H_2S was not formed directly from the sulfur compound, but from the sulfur on the catalyst. It has also been proposed that only sulfur bonded to both Ni and Mo is labile [48]. The removal of H_2S will form a new vacancy on the catalyst. Thus, a shift of vacancy on the catalyst surface would occur.

The catalysts show high activity for the hydrodesulfurization of thiophene, particularly the sulfided NiMo–AlZrP catalysts, which exhibit in comparison a higher activity than Ni, Mo and NiMo sulfided catalysts supported on carbons [50], zeolites [51] and alumina pillared smectites [17], tested in similar conditions.

The regeneration of spent catalyst was performed by passing a 5% (v/v) O_2/N_2 mixture at a flow rate of 60 cm^3/min through the reactor, while the temperature was raised from room temperature to 673 K at a rate of 10 K/min. The final temperature was maintained for 2 h, and the reactor was cooled to room

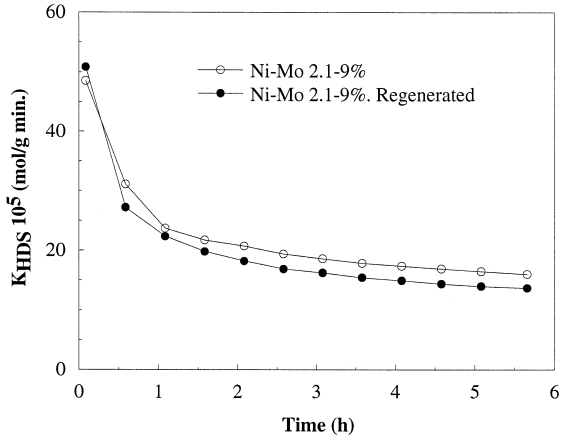

Fig. 12. Effect of the regeneration treatment on the thiophene HDS catalytic activity.

temperature in a flow of 5% (v/v) O_2/N_2 mixture. Fig. 12 shows that a total regeneration of the catalysts was reached, meaning that the structure is not affected in this process, by either segregation or diffusion of the active components of the catalyst.

Finally, it is noticeable the different selectivities of these catalysts, thus Ni-based does not produce butane as a hydrogenation product of reaction. The hydrogenation ability of the catalyst can be interpreted by the presence of active hydrogen, furthermore, the hydrogenation activity is higher for transition metal sulfides whose structure enables the formation of intercalated compounds, such as MoS_2. Hydrogen activation takes place through intercalation in MoS_2, that is by proton permeation in the van der Waals gap and by stabilising the electron charge in the 2p-band of sulfur [52,53]. The edge sites are suitable for alkene adsorption during hydrogenation or isomerization reactions [54].

5. Conclusions

Fluorinated alumina pillared α-zirconium phosphate materials have shown to be appropriate supports for preparing sulfided catalysts. The Ni–Mo oxides precursors revealed to be active in the HDS reaction of thiophene, which means that there is an in situ sulfidation of the oxidic phase. The Ni-based catalysts have promising activities which are sustained for a long time, and may be increased when the formation of the oxidic phase was obtained at a lower temperature (623 K) in this way avoiding the formation of a spinel structure on the nanostructured alumina. Interestingly, these compounds are not active for hydrogenation reactions and the products of reaction of thiophene are exclusively butenes. The Ni–Mo based catalysts are highly dispersed and the most active phases, with K_{HDS} values higher than 2×10^{-4} mol/g min (after 300 min) owing to the promoter effect of Ni. In addition, regeneration of the catalysts could be achieved by treatment with 5% (v/v) O_2/N_2 at 673 K without loss of activity.

Acknowledgements

This research was supported by CICYT (Spain) Proyect MAT97-906 and by E.U. Programme BRIT-EURAM Contract BRE2-CT-93-0450.

References

[1] O. Weisser, S. Landa, Sulphide Catalysts, Their Properties and Applications, Pergamon, New York, 1973.
[2] F.E. Massoth, in: Advances in Catalysis and Related Subjects, Vol. 27, Academic Press, New York, 1978, p. 265.
[3] B. Delmon, in: H.F. Barry, P.C.H. Mitchell (Eds.), Proceedings, 3rd International Conference on the Chemistry and Uses of Molybdenum, Climax Molybdenum, Ann Arbor, 1979, p. 73.
[4] P. Grange, Catal. Rev. Sci. Eng. 21 (1980) 135.
[5] P. Ratnasamy, S. Sivasanker, Catal. Rev. Sci. Eng. 22 (1980) 401.
[6] B.C. Gates, J.R. Katzer, G.C.A. Schuit, Chemistry of Catalytic Processes, McGraw-Hill, New York, 1979, p. 390.
[7] R. Cid, J. Neira, J. Godoy, J.M. Palacios, A. López-Agudo, Appl. Catal. A: General 125 (1995) 169.
[8] R. Cid, J. Neira, A. López-Agudo, Bol. Soc. Chil. Quim. 40 (1995) 371.
[9] R. Cid, S. Bendezu, J. Godoy, A. López-Agudo, Bol. Soc. Quim. 40 (1995) 135.
[10] Y. Okamoto, H. Tomioka, T. Imanaka, S. Teranshi, J. Catal. 66 (1980) 93.
[11] J. Olorunyolemi, R. Kydd, J. Catal. 158 (1996) 583.
[12] M. Wu, D.M. Hercules, J. Phys. Chem. 83 (15) (1979) 2003.
[13] B. Scheffer, P. Molhock, J.A. Moulijn, Appl. Catal. 46 (1989) 11.
[14] A. Gil, A. Díaz, L.M. Gandía, M. Montes, Appl. Catal. A 109 (1994) 167.
[15] L.M. Gandía, M. Montes, J. Mol. Catal. 94 (1994) 347.
[16] L.M. Occelli, R.J. Rennard, Catal. Today 2 (1988) 309.
[17] J.T. Kloprogge, W.J.J. Welters, E. Booy, V.H.J. de Beer, R.A. van Sante, J.W. Geus, J.B.H. Jansen, Appl. Catal. A 97 (1993) 77.
[18] J. Mérida-Robles, P. Olivera-Pastor, A. Jiménez-López, E. Rodríguez-Castellón, J. Phys. Chem. 100 (35) (1996) 14726.
[19] J. Mérida-Robles, P. Olivera-Pastor, E. Rodríguez-Castellón, A. Jiménez-López, J. Catal. 169 (1997) 317.
[20] J.F. Moulder, W.F. Stickle, P.E. Sobol, K.D. Bombeu, in: J. Chastain (Ed.), Handbook of X-Ray Photoelectron Spectroscopy, Perkin-Elmer, 1992.
[21] P. Arnoldy, J.C.M. de Jongue, J.A. Moulijn, J. Phys. Chem. 89 (1985) 4517.
[22] Y.J. Huang, J.A. Schwarz, Appl. Catal. 36 (1988) 163.

[23] L. Daza, B. Pawelec, J.A. Anderson, J.L.G. Fierro, Appl. Catal. A 87 (1992) 145.
[24] B. Scheffer, P.J. Magnus, J.A. Moulijn, J. Catal. 121 (1990) 18.
[25] R. Burch, A. Collins, J. Catal. 97 (1986) 385.
[26] Y. Okamoto, H. Nakano, T. Shimakawa, J. Catal. 50 (1977) 447.
[27] A. Arteaga, J.L.G. Fierro, F. Delannay, B. Delmon, Appl. Catal. 26 (1986) 227.
[28] S. Mendioroz, J.M. Palacios, J.L.G. Fierro, A. López-Agudo, Bull. Soc. Chim. Belg. 96 (1987) 891.
[29] J.W.E. Coenen, Appl. Catal. 75 (1991) 193.
[30] J.M. Rynkowski, T. Paryjczal, M. Lenik, Appl. Catal. 106 (1993) 73.
[31] Ch. Minchev, V. Knarizer, L. Kosova, V. Pechev, W. Grunsser, F. Schimidt, in: L.V.C. Rees (Ed.), Proceedings 5th Conference on Zeolites, Heyden, London, 1980, p. 335.
[32] M. Suzuki, K. Tsutsumi, H. Takahashi, Zeolites 2 (1982) 87.
[33] T. Rosenquist, J. Iron Steel Inst. 176 (1954) 37.
[34] P.J. Magnus, PhD Thesis, University of Amsterdam, The Netherlands, 1989.
[35] S.P.A. Louwers, R. Prins, J. Catal. 133 (1992) 94.
[36] R. Burch, A. Collins, Appl. Catal. 18 (1985) 373.
[37] Y. Okamoto, A. Maezawa, T. Imanaka, J. Catal. 120 (1989) 29.
[38] P. Ratnasamy, S. Sivasanker, Catal. Rev. Sci. Eng. 22 (1980) 401.
[39] B.S. Clausen, B. Lengeler, R. Candia, J. Als-Nielsen, H. Topsoe, Bull. Soc. Chim. Belg. 90 (1981) 1249.
[40] H. Topsøe, B.S. Clausen, N.-Y. Topsøe, E. Pedersen, W. Niemann, A. Müller, H. Bögge, B. Lengeler, J. Chem. Soc. Faraday Trans. 83 (1987) 2157.
[41] N.-Y. Topsøe, H. Topsøe, F.E. Massoth, J. Catal. 119 (1989) 252.
[42] I. Alstrup, L. Chorkendorff, R. Candia, B.S. Clusen, H. Topsoe, J. Catal. 77 (1982) 397.
[43] U.S. Ozkan, L. Zhang, S. Ni, E. Moctezuma, J. Catal. 148 (1994) 181.
[44] L. Blanchard, J. Grimblot, J.P. Bonnelle, J. Catal. 98 (1986) 229.
[45] T. Kabe, W. Qian, S. Ogawa, A. Ishihara, J. Catal. 143 (1993) 239.
[46] W. Qian, A. Ishihara, S. Ogawa, T. Kabe, J. Phys. Chem. 98 (1994) 907.
[47] T. Kabe, W. Qian, A. Ishihara, J. Phys. Chem. 98 (1994) 912.
[48] T. Kabe, W. Qian, A. Ishihara, J. Catal. 149 (1994) 171.
[49] S.H. Yang, C.N. Satterfield, J. Catal. 81 (1983) 168.
[50] S. Eijsbouts, J.N.M. van Gestel, E.M. van Oers, R. Prins, J.A.R. van Veen, V.H.J. de Beer, Appl. Catal. A: General 119 (1994) 293.
[51] W.J. Welters, G. Vorbeck, H.W. Zandbergen, J.W. de Haan, V.H.J. de Beer, R.A. van Sante, J. Catal. 150 (1994) 155.
[52] R. Schollhorn, M. Kumpersand, D. Plorin, J. Less-Common Met. 58 (1978) 55.
[53] R. Schollhorn, Angew. Chem. 92 (1980) 1015.
[54] A. Andreev, Ch. Vladov, L. Phahov, P. Atanasova, Appl. Catal. A: General 108 (1994) 97.